Dynamic Simulation and Optimization for *Arthrospira platensis* Growth and C-phycocyanin Production

Ehecatl Antonio del Rio-Chanona[1,‡], Dongda Zhang[1,‡,*], Youping Xie[4], Emmanuel Manirafasha[2], Keju Jing[2,3,*]

[1]Department of Chemical Engineering and Biotechnology, University of Cambridge, Pembroke Street, Cambridge CB2 3RA, UK.

[2]Department of Chemical and Biochemical Engineering, College of Chemistry and Chemical Engineering, Xiamen University, Xiamen 361005, China

[3]The Key Lab for Synthetic Biotechnology of Xiamen City, Xiamen University

[4]College of Biological Science and Engineering, Fuzhou University, Fuzhou 350108, China

[‡]: These authors contributed equally to this work.

[*]: corresponding author, email: dz268@cam.ac.uk (Dongda Zhang), tel: (+441223) 330132; jkj@xmu.edu.cn (Keju Jing), tel: 86 592 2186038.

Abstract

C-phycocyanin is a high-value bioproduct synthesized from cyanobacterium *Arthrospira platensis*. To facilitate its application, advanced dynamic models were built to simulate the complex effects of light intensity, light attenuation and nitrate concentration on cell growth and pigment production in the current research. By comparing these models against the experimental results, their accuracy was verified in both batch and fed-batch processes. Three key findings are presented in this work. First, a noticeable difference between the optimal light intensity for cell growth (282 μmol m^{-2} s^{-1}) and phycocyanin synthesis (137 μmol m^{-2} s^{-1}) is identified. Second, light attenuation is demonstrated to be the primary factor causing the decrease of intracellular phycocyanin content instead of nitrate concentration in the fed-batch process, while it has no significant effect on total phycocyanin production. Finally, although high nitrate concentration can enhance cell growth, it is demonstrated to suppress intracellular phycocyanin accumulation in a long-term operation.

Keywords: C-phycocyanin production; *Arthrospira platensis* cultivation; fed-batch operation; dynamic simulation; light attenuation; photobioreactor.

1. Introduction

C-phycocyanin is a blue antenna pigment, mainly used to enhance the photosynthetic efficiency of cyanobacteria and red algae [1,2]. It has been considered as a high-value bioproduct due to its wide applications in different industries [3]. For example, it is currently utilized as a natural colorant to replace other toxic synthetic pigments in both food and cosmetic production [4]. It also shows great potential for the pharmaceutical industry due to its unique anti-oxidant, neuroprotective and anti-inflammatory properties [4,5].

At present, there are different microorganisms capable of producing C-phycocyanin. Amongst several candidates, *Arthrospira platensis* (*A. platensis*), a type of cyanobacteria, has been selected as the primary species for C-phycocyanin production due to its high phycocyanin content which is up to 15% of the cell's dry weight [2,6]. Furthermore, *A. platensis* cultivation has been industrialized in several countries as this specie contains many high-value chemicals such as carotenoids and γ-linolenic acid, and can be served as a food supplement [3,7], which further increases its desirability.

Despite the remarkable properties of *A. platensis*, its low biomass concentration and phycocyanin productivity achieved in large-scale open ponds and photobioreactors (PBRs) severely prevent the further commercialization of phycocyanin production. For example, the biomass density of *A. platensis* can hardly go beyond 0.8 g L^{-1} and phycocyanin content is only around 7% of the cell dry weight [1,8–10]. In order to enhance biomass concentration and maximize phycocyanin production, it is essential to implement dynamic control and

optimization techniques. These strategies have been demonstrated to have significant positive impact in the performance of both laboratory and industrial scale bioprocesses [11–15].

Nonetheless, to successfully execute dynamic control and optimization it is necessary to build a dynamic model capable of accurately predicting the behavior of the biosystem. Despite its importance, very little effort has been invested in researching this aspect. Although a few models have been proposed by previous research, they do not include the influence of either light intensity or nutrient concentration on cell growth and phycocyanin production, and thus are not applicable for future process design [6,8].

For example, previous research declared that *A. platensis* growth rate increases with increasing light intensity from 75 μmol m^{-2} s^{-1} to 300 μmol m^{-2} s^{-1}, beyond which photo-inhibition can be observed (450 μmol m^{-2} s^{-1}) and cell growth terminates [2]. On the contrary, phycocyanin synthesis was found to be suppressed in a higher light intensity, and its content drops from 15% of cell dry weight to less than 10% of cell dry weight when light increases from 75 μmol m^{-2} s^{-1} to 300 μmol m^{-2} s^{-1} [2,3].

Therefore, to address this open challenge, the current work aims to build an accurate model capable of simulating the entire process for both cell growth and phycocyanin accumulation. Specifically, the essential factors included in the current research are nutrient concentration, light attenuation and light intensity. Although temperature is also known to be an important factor affecting pigment synthesis and cell growth, previous research has found that suitable

temperature for cell growth is located in a narrow range from 25 ℃ to 30 ℃ [16]. Thus temperature is always fixed in experiments and not included in the current study.

2. Model construction theory

In the current study, two models are modified based on the original Monod and Droop models. Experimental data from three batch processes is used to estimate the model parameters, and two additional fed-batch processes are used for the verification of model accuracy (predictive ability).

2.1 Experimental setup

Three batch processes have been performed in our previous work [2]. In these experiments, *A. platensis* WH879 was selected for phycocyanin production, and temperature was kept at 28℃. A 1 L photobioreactor (15.5 cm in length and 9.5 cm in diameter) was used in the batch processes with an external light source mounted on both sides. Initial biomass and nitrate concentrations in the three experiments were kept constant, and incident light intensities were set at 75 μmol m^{-2} s^{-1}, 150 μmol m^{-2} s^{-1} and 300 μmol m^{-2} s^{-1}, respectively. All the processes lasted for more than two weeks until nitrate was consumed.

To extend cell growth and enhance phycocyanin production, two fed-batch processes were carried out with a fixed incident light intensity of 300 μmol m^{-2} s^{-1} and temperature of 28℃. Nitrate concentration in the reactor was intermittently replenished, to 5 mM in one process (named as 5 mM fed-batch process) and to 10 mM in the other (named as 10 mM fed-batch

process), after the initial nitrate was depleted. Both processes were continued for 13 days and stopped when phycocyanin content in cells commenced to decrease. The detailed introduction to experiment design and measurement techniques can be found in our previous work [2].

2.2 Model construction

During the batch experiments, cell growth underwent two types of conditions, nitrate-sufficient at the beginning of the processes and nitrate-limiting at the end of the experiments. Phycocyanin content decreased remarkably after nitrate becomes a limiting nutrient (1.4 mM, less than 10% of the initial concentration). This happens because phycocyanin is an intracellular nitrogen storage which can be consumed by cells in nitrogen-free conditions [1]. Therefore, understanding the change of intracellular nitrogen concentration is clearly important for the phycocyanin production process.

The decline of phycocyanin content was also observed in both fed-batch processes after biomass concentration went up to 6 g L^{-1}, although nitrate was always replenished. As phycocyanin is an antenna pigment that increases the efficiency of cyanobacterial photosynthesis, lower illumination intensity is preferable for phycocyanin accumulation [3]. On the other hand, if light intensity is too low for *A. platensis* to process photosynthesis, phycocyanin can also be converted to other nitrogen storage for cell maintenance [3,4].

Moreover, it is notable that during the fed-batch experiments since intracellular nitrogen concentration was not measured, it is difficult to exclude the possibility that cells were

nitrogen-starved in the final period of the experiments. Therefore, to explore the effects of nitrate concentration and light intensity on cell growth and phycocyanin production, and to identify the primary limiting factor for phycocyanin accumulation in the fed-batch processes, two types of dynamic models are built in the current work as will be explained in Sections 2.2.1 and 2.2.2.

2.2.1 The Monod model

The Monod model has been widely applied to describe microorganism growth in nutrient-sufficient cultures, where intracellular nutrient concentration is kept constant because of the rapid replenishment [17]. Since nitrate is available in most of the running time of our batch processes, the Monod model is selected in the current study, as shown in Equations (1a) to (1d).

$$\frac{dc_X}{dt} = r_M \cdot c_X - u_d \cdot c_X \quad (1a)$$

$$\frac{dc_N}{dt} = -Y_{N/X} \cdot r_M \cdot c_X \quad (1b)$$

$$\frac{d\left(c_{q_cX}\right)}{dt} = k \cdot c_X - \frac{k_d \cdot c_{q_cX}}{c_N + K_{Np}} \quad (1c)$$

$$r_M = u_0 \cdot \frac{c_N}{c_N + K_N} \quad (1d)$$

where c_X is biomass concentration, u_0 is maximum cell specific growth rate, r_M is cell specific growth rate, c_N is nitrate concentration, K_N is nitrate limitation constant, K_{Np} is nitrate limitation constant for phycocyanin consumption, u_d is cell specific decay rate, $Y_{NO_3/X}$ is nitrate yield coefficient, q_c is phycocyanin content in cells, c_{q_cX} is phycocyanin concentration in the culture, k is phycocyanin production constant and k_d is phycocyanin

consumption constant.

In Equation (1a), u_0 is a function of light intensity and will be fully introduced later; u_d is assumed to be constant since a previous study has found it to be independent from light intensity [18]. In Equation (1b), it is assumed that the nitrate consumption rate is determined by cell growth rate (r_M) and independent from cell decay rate, since nitrate is predominantly consumed for cell growth. Therefore, cell decay rate, u_d, is not included in this equation. Recent research has demonstrated that phycocyanin production rate is proportional to biomass concentration, but that it is not seriously affected by cell growth rate [6]. Therefore, in Equation (1c) $k \cdot X$ is used to simulate the effect of biomass concentration on phycocyanin production.

Since phycocyanin is an intracellular nitrogen storage which can be consumed for cell maintenance in nitrate-limiting conditions, a consumption term has to be embedded in Equation (1c). Due to the fact that no research has focused on the relation between phycocyanin consumption rate and cell growth rate, the current study assumes first-order kinetics to approximate phycocyanin consumption rate, as shown in the second term on the right of Equation (1c). It is also assumed that phycocyanin consumption rate depends on the nitrate concentration in the culture. Similar with Equation (1a), it is assumed that in Equation (1c) the phycocyanin production constant, k, depends on light intensity and its expression will be presented later.

2.2.2 The Droop model

Intracellular nitrogen concentration is important for phycocyanin biosynthesis, however, the Monod model does not take into account this factor. Therefore, the Droop model is selected in the present study to compare with the Monod model. Equations (2a) to (2d) show the Droop model.

$$\frac{dc_X}{dt} = r_D \cdot c_X - u_d \cdot c_X \quad (2a)$$

$$\frac{dc_N}{dt} = -Y_{N/X} \cdot r_M \cdot c_X \quad (2b)$$

$$\frac{dc_q}{dt} = Y_{q/X} \cdot r_M - u_0 \cdot r_D \cdot c_q \quad (2c)$$

$$\frac{dc_{q_c}}{dt} = k \cdot \left(1 - \frac{k_q}{c_q}\right) - \frac{k_d}{c_q} \quad (2d)$$

$$r_D = u_0 \cdot \left(1 - \frac{k_q}{c_q}\right) \quad (2e)$$

where k_q is minimum normalised nitrogen quota, c_q is normalised nitrogen quota and $Y_{q/X}$ is nitrogen quota yield coefficient.

The Droop model assumes that microorganism growth directly depends on the intracellular nutrient concentration rather than the extracellular nutrient concentration in the culture [17]. Thus in a nutrient-limiting or nutrient-deplete culture, microorganisms can keep growing by consuming the intracellular stored nutrient until it drops to the minimum quota. Given that in our experiments intracellular nitrogen concentration was not measured, a normalized intracellular nitrogen concentration (normalized nitrogen quota) is used. This is defined as the ratio of intracellular nitrogen concentration during the experiments to the intracellular nitrogen

concentration at the beginning of the experiments [19]. In Equation (2d), the first term on the right represents the phycocyanin production rate, which is assumed to be a function of intracellular nitrogen sufficiency, and the second term represents the phycocyanin consumption rate which is assumed inversely proportional to the nitrogen quota. u_0 and k are also functions of light intensity as is the case in the Monod model.

2.2.3 Modelling of light intensity effects (PI-curve)

There exists an optimal light intensity for cyanobacteria growth, below which cell growth rate increases with the increasing light intensity, and above this level the cell growth rate decreases with the increasing light intensity. To accurately represent accurately photo-limitation, photo-saturation, and photo-inhibition phenomena, the Aiba model has been extensively used in recent studies and is shown in Equation (3) [20]. Based on this model, the optimal light intensity for biomass growth can be calculated to be $\sqrt{k_s \cdot k_i}$, as it maximizes the value of biomass specific growth rate (u_0). The detailed derivation of optimal light intensity is shown in the Supporting Information. Similarly, an optimal light intensity also exists for phycocyanin accumulation and the effect of illumination intensity on phycocyanin synthesis can be expressed in Equation (4). The optimal illumination for phycocyanin synthesis based on Equation (4) is $\sqrt{k_{sp} \cdot k_{ip}}$.

$$u_0(I(z)) = u_m \cdot \frac{I(z)}{I + k_s + \frac{I^2}{k_i}} \tag{3}$$

$$k(I(z)) = k_m \cdot \frac{I(z)}{I + k_{sp} + \frac{I^2}{k_{ip}}} \tag{4}$$

where u_m is the maximum specific growth rate, k_m is the maximum phycocyanin accumulation constant, I is light intensity, k_s and k_{sp} are light saturation terms for cell growth and phycocyanin synthesis, respectively. k_i and k_{ip} are light inhibition terms for cell growth and phycocyanin synthesis, respectively.

Furthermore, due to the severe light attenuation observed in the current PBR, local light intensities that cells experience are much lower than the incident light intensity. To take into account this phenomenon, the modified Lambert-Beer's law has been selected and shown in Equation (5) [21]. This equation includes the two main factors causing light attenuation in PBRs, namely bubble scattering and cell absorption.

$$I(z) = I_0 \cdot \left(e^{-(\tau \cdot X + K_a) \cdot z} + e^{-(\tau \cdot X + K_a) \cdot (L - z)}\right) \quad (5)$$

where I_0 is incident light intensity, τ is cell absorption coefficient, K_a is bubble reflection coefficient, z is the distance from light source and L is the width of the PBR.

Another issue arising when implementing Equations (3) to (5) into the current models is that the models will contain one spatial dimension and one temporal dimension, which indicates that they will become partial differential equations. To facilitate parameter estimation process and further dynamic simulation, μ-integration and phycocyanin production rates were estimated by the 10-step Trapezoidal rule shown in Equations (6a) and (6b) [22]. In order to simplify the complexity of the models, the current tank PBR is assumed to be a column with a square cross section. The square area is assumed to be the same as the circle area, which means

the length of the square is 8.40 cm.

$$u_0 = \frac{u_m}{20} \cdot \sum_{n=1}^{9} \left(\frac{I_{i=0}}{I_{i=0} + k_s + \frac{I_{i=0}^2}{k_i}} + 2 \cdot \frac{I_{i=\frac{n \cdot L}{10}}}{I_{i=\frac{n \cdot L}{10}} + k_s + \frac{I_{i=\frac{n \cdot L}{10}}^2}{k_i}} + \frac{I_{i=L}}{I_{i=L} + k_s + \frac{I_{i=L}^2}{k_i}} \right) \quad (6a)$$

$$k = \frac{k_m}{20} \cdot \sum_{n=1}^{9} \left(\frac{I_{i=0}}{I_{i=0} + k_{sp} + \frac{I_{i=0}^2}{k_{ip}}} + 2 \cdot \frac{I_{i=\frac{n \cdot L}{10}}}{I_{i=\frac{n \cdot L}{10}} + k_{sp} + \frac{I_{i=\frac{n \cdot L}{10}}^2}{k_{ip}}} + \frac{I_{i=L}}{I_{i=L} + k_{sp} + \frac{I_{i=L}^2}{k_{ip}}} \right) \quad (6b)$$

2.2.4 Parameter estimation methodology

Accurate estimation of parameters is a critical task within model construction, as unreliable parameters can seriously restrict the potential applications of models for evaluation and design purposes. To estimate the parameters in both models, a nonlinear least-squares optimization problem is formulated [19]. The dynamic models are discretised and transformed into nonlinear programming problems (NLPs). Given the high nonlinearity and stiffness of the differential equation models, orthogonal collocation over finite elements in time is used as a discretization scheme. The optimal parameters for the underlying model are determined by solving the NLP using the state-of-the-art interior point nonlinear optimization solver IPOPT [23].

The implementation in this work is programmed in the Python optimization environment Pyomo [24]. Pyomo is a tool package for modelling optimization applications in Python and serves as an interface for the optimization solver IPOPT. This strategy constitutes a very efficient and accurate procedure to estimate parameters of highly nonlinear dynamic processes

[25]. The dynamic models are simulated in Wolfram *Mathematica*® 10.

3. Results and discussion

3.1 Parameter estimation result

Parameter values in the Monod model are shown in Table 1, and those in the Droop model are shown in Table 2. Figure 1 shows the simulation results of both models and the experimental results in the batch processes. From Figure 1 it can be seen that both models represent experiments well, which indicates that both the parameter estimation methodology and the dynamic models proposed in the current study are accurate.

However, both of the models are not able to fit the cyanobacterial stationary phase at the very end of the batch process in which incident light intensity is 75 μmol m^{-2} s^{-1}. One potential reason is that average light intensity in the reactor at the end of this experiment is too low (around 10 μmol m^{-2} s^{-1}, estimated based on Equation (5)) for cells to activate photosynthesis, and the Aiba model cannot be applied in such a weak illumination region [26].

3.2 Verification of model accuracy

Despite the good fitting of both models, it is necessary to further verify the accuracy of both models when used to predict the performance of unknown processes. The model predictability is particularly important in the current work since its goal is to build accurate dynamic models to implement process control and optimization for the underlying process, and to identify the limiting factors for phycocyanin production in different operation modes. As a result, both

models are utilized to simulate the two fed-batch processes.

Figure 2 shows the comparison of simulation results and experimental results. From Figures 2(a) and 2(b), it is clear that the Monod model successfully predicts the biomass concentration during the entire time-course of both fed-batch processes, while the Droop model predicts a much lower biomass concentration compared to the experimental results. Both models are in good agreement with the experimental results for nitrate concentration (shown respectively in Figures 2(c) and 2(d)). Although both models underestimate phycocyanin production, the Monod model compared to the Droop model shows a much better trend and closer simulation results to the experimental measurements, especially in the 10 mM nitrate feeding fed-batch process (Figures 2(e) and 2(f), respectively).

It is notable that the Monod model assumes a nitrate-sufficient condition where intracellular nitrogen concentration is always sufficient and does not limit cell growth or pigment synthesis. However, the Droop model assumes a nitrate-limiting condition where intracellular nitrogen concentration is a limiting factor for cell growth and nitrogen storage, such that phycocyanin has to be converted to other proteins for biomass maintenance. In the current study, as nitrate concentration was kept between 2.4 mM to 5.0 mM in the 5 mM fed-batch process, it is possible that the culture is temporally subject to a nitrate-limiting condition. However, since the number and nature of the parameters in both models are similar, the much better prediction produced by the Monod model indicates that in both fed-batch processes nitrate concentrations are always sufficient and do not limit cell growth. As a result, the decrease of phycocyanin content

in fed-batch processes should be ascribed to other reasons such as low local light intensity instead of nitrate concentration.

Overall, as the Monod model is found to represent very adequately the results of three batch experiments and to predict accurately the performance of two fed-batch processes, it is selected for further study. Based on the Monod model, the optimal light intensity for cell growth and phycocyanin accumulation without light attenuation is calculated to be 282 μmol m^{-2} s^{-1} and 137 μmol m^{-2} s^{-1}, respectively. This conclusion is also consistent with a previous study which observed an increase of 27% on phycocyanin content when illumination decreases from 1100 μmol m^{-2} s^{-1} to 100 μmol m^{-2} s^{-1} [4].

3.3 Light attenuation effects on cell growth and phycocyanin accumulation

To further study the influence of light attenuation on phycocyanin production, the first 200 hours of the 10 mM nitrate feeding fed-batch process are used in this section since the nitrate concentration is not a limiting factor (700 mg L^{-1}) and its effects on cell growth and phycocyanin synthesis are negligible. Figure 3 shows the local light intensity, cell growth rate, phycocyanin accumulation rate in cells and phycocyanin production rate in the culture at different biomass concentrations.

From Figure 3(a), it can be clearly observed that light intensity distribution is uniform at the beginning of the process due to the low biomass concentration, while light attenuation becomes severe only after 50 hours when biomass concentration increases to 1.50 g L^{-1} (Figure 3(b))

where biomass absorption becomes significant. This observation is consistent with a recent study [27] which found that cyanobacteria concentration higher than 1.80 g L^{-1} can introduce a severe light attenuation in a photobioreactor. In the late period of the process (200^{th} hour) light is not able to penetrate the whole volume of the vessel (Figure 3(a)), and the majority of the PBR is in the dark zone where photosynthesis is unable to progress.

Because of the non-uniformity of the local illumination distribution, a cyanobacterial exponential growth phase (where cell growth rate increases with increasing biomass concentration) can be found in the outer sides of the reactor (Figure 3(b)). This is because both nutrients and illumination are sufficient. However, in the central part of the reactor, cell growth rate initially does not change much during the first 50^{th} hours due to the uniform light distribution, but decreases rapidly to zero (Figure 3(b)) at the end of the experiment due to the severe light attenuation (Figure 3(a)) which causes a low local light intensity and prevents cyanobacteria photosynthesis. Therefore, the increase of biomass concentration in the process is mainly attributed to the biomass exponential growth in the light zone.

Compared to cell growth, phycocyanin accumulation is more complicated. Although the incident light intensity is close to the optimal value for cyanobacterial growth, it is much higher than that for phycocyanin synthesis. Therefore, during the initial period photo-inhibition dominates the entire volume of the reactor for phycocyanin synthesis, and phycocyanin accumulation rate is slightly higher in the middle part of the reactor where the local light intensity is lower (Figure 3(c)). The average phycocyanin accumulation rate in this period is

high because phycocyanin content in cells is much lower than the saturation content, which suppresses the phycocyanin consumption rate. With the increasing biomass concentration, at the 50^{th} hour local light intensity in the inner part of the reactor reduces to around 100 μmol m^{-2} s^{-1} which is close to the optimal intensity for phycocyanin synthesis. Hence, local phycocyanin accumulation rate in this part (photo-saturation zone) is kept high because of the suitable illumination intensity (Figure 3(c)).

On the contrary, phycocyanin accumulation rate decreases remarkably and becomes negative in the outer sides of the reactor, as these locations are in proximity to light sources and cyanobacteria do not need high phycocyanin content under high illumination intensity. Because the culture is well-mixed, cells which have accumulated a high content of phycocyanin in the middle part of the PBR will commence to consume phycocyanin when they move to the photo-inhibition zone (outer sides) of phycocyanin synthesis.

With further increase in the biomass concentration, during the final period of the experiment the photo-saturation zone for phycocyanin synthesis moves to the outer sides and phycocyanin accumulation terminates in the middle part of the reactor because of the low local illumination (Figure 3(c)). Due to the severe light attenuation, cells in the middle part of the reactor start to convert phycocyanin to other nitrogen storage as they cannot perform photosynthesis. From Figure 3(c) it can be found that at the 200^{th} hour photo-limitation dominates the major volume of the reactor and photo-inhibition controls the outer sides of the PBR. Even in the photo-saturation zone phycocyanin accumulation rate is lower than before, as phycocyanin has

accumulated almost 3 times as much as at the beginning of the process and approaches to saturation.

Different to phycocyanin accumulation trend in the reactor, phycocyanin production rate in the outer sides increases significantly during the whole fed-batch process (Figure 3(d)). This is because the decrease of phycocyanin content in cell can be totally offset by the increase of biomass concentration, as phycocyanin production is the product of biomass concentration and phycocyanin content in cells. Only during the final period of the process the local phycocyanin production rate in the central part of the reactor decreases to zero, or even slightly below, since both cell growth and phycocyanin accumulation have been terminated in the low illumination condition and phycocyanin is converted to other nitrogen storage. As a result, although phycocyanin content has decreased, total phycocyanin production may still be enhanced in the final period of the process.

3.4 Nitrate concentration effects on phycocyanin accumulation

Although nitrate is essential for phycocyanin accumulation and a nitrate-sufficient culture can help to maintain a high content of phycocyanin in cells, its excess will aggravate the local light intensity distribution since biomass concentration can be significantly enhanced. For example, if the initial nitrate concentration in the 10 mM nitrate feeding fed-batch process increases by 20%, based on the current simulation a slightly lower phycocyanin content in cells will be obtained in the experiment (reduced by 4.5%), even though this decrease does not affect phycocyanin production because of the higher biomass concentration (increased by 5.5%). This

conclusion also explains the experimental observations in previous research where lower nitrate concentrations in fed-batch process are favorable for phycocyanin and other photosynthetic pigments accumulation [2,28].

Moreover, the poor local light distribution caused by the excess of nitrate can lead the majority of the volume of the reactor to a photo-limitation condition, which will inevitably reduce the photobioreactor efficiency as phycocyanin cannot be synthesized in most part of the reactor. At present, as the design of highly efficient photobioreactors is one of the major challenges preventing the industrialization of high-value bioproduct production processes, it is important to provide optimal operating conditions to guarantee the high efficiency of future photobioreactors.

As a result, based on the current model it can be concluded that although nitrate is necessary for phycocyanin synthesis, always maintaining a nitrate-sufficient culture may not be a sensible strategy for phycocyanin production. Even though total phycocyanin production is not highly affected by the addition of nitrate in the reactor, the decrease of final phycocyanin content in cells may become an issue to prevent the industrialization of this process, since the phycocyanin downstream separation cost can be significantly increased.

4. Conclusion

This contribution presents the detailed modelling of *A. platensis* growth and phycocyanin production. Based on the models developed, the limiting factor for phycocyanin production in

a fed-batch process was identified. By estimating the optimal light intensities for cell growth and phycocyanin accumulation, the current work proved the previous hypothesis that a lower light intensity is preferable for phycocyanin synthesis. Moreover, the present study also illustrated the unexplained experimental observation [2,4] that a lower nitrate concentration can enhance the final phycocyanin content in a fed-batch process.

To facilitate the industrialization of this process, effects of other nutrients such as phosphate and Fe on cell growth and phycocyanin synthesis can also be carried out following the same procedure presented in the current study. In addition, three aspects can be directly explored in future work based on the current model.

First, as the current work has demonstrated, precisely controlling nitrate concentration is necessary for the improvement of phycocyanin production. Hence, the present model can be used to control the addition of nitrate concentration for future experimental processes. In particular, advanced process optimization techniques such as model predictive control should be implemented to estimate the optimal nitrate feeding rate and incident light intensity in a fed-batch process, so that the phycocyanin production can be maximized and meanwhile the high phycocyanin content can be guaranteed. What is more, model predictive control can also improve the accuracy of current model since parameters in the dynamic model can be synchronized with the ongoing process in this technique. Thus the model accuracy can be always guaranteed.

Second, since light attenuation inside of photobioreactors always plays an important role to limit the efficiency of photo-fermentation processes, the present model can be used to simulate the light transmission performance in different configurations of photobioreactors so that suitable configurations for large scale photobioreactor design can be eventually identified. Moreover, continuous process can be designed based on the current model. As biomass concentration in a continuous process is in general constant, light attenuation will not be aggravated with the ongoing process. Thus the effect of light attenuation on cell growth and pigment accumulation can be solved.

Third, the current dynamic model is built based on a laboratory scale photobioreactor in which culture is well-mixed and interphase mass transfer from gas to liquid is rapid. However once the reactor is scaled up, both mass transfer and culture homogeneity can become severe limiting factors for biomass cultivation and phycocyanin production. Therefore, to guarantee the high accuracy of the current model in large scale process simulation, kinetic equations estimating the gas mass transfer and consumption rate should also be embedded in the current model in further work.

Acknowledgement

Author E. A. del Rio-Chanona is funded by CONACyT scholarship No. 522530 and the Secretariat of Public Education and the Mexican government. This work was also supported by the National High Technology Research and Development Program 863, China (No.

2014AA021701) and the National Marine Commonwealth Research Program, China (No. 201205020-2).

Supporting Information Statement

The supporting information contains the derivation of optimal light intensity for cell growth and bioproduct synthesis from the Aiba model. This information is available free of charge via the Internet at http: //pubs.acs.org.

Nomenclature

c_X	biomass concentration
u_0	cell specific growth rate
c_N	nitrate concentration
K_N	nitrate limitation constant
K_{Np}	nitrate limitation constant for phycocyanin consumption
u_d	cell specific decay rate
$Y_{NO_3/X}$	nitrate yield coefficient
c_{q_c}	phycocyanin content in cells
k	phycocyanin production constant
k_d	phycocyanin consumption constant
k_q	minimum normalized nitrogen quota
c_q	normalized nitrogen quota
$Y_{q/X}$	nitrogen quota yield coefficient
u_m	maximum specific growth rate
k_m	maximum phycocyanin accumulation constant
I	light intensity
k_s	light saturation terms for cell growth
k_{sp}	light saturation terms for phycocyanin synthesis
k_i	light inhibition terms for cell growth
k_{ip}	light inhibition terms for phycocyanin synthesis
I_0	incident light intensity

τ	cell absorption coefficient
K_a	bubble reflection coefficient
z	distance from light source
L	width of the PBR

References

(1) Eriksen, N. T. Production of Phycocyanin--a Pigment with Applications in Biology, Biotechnology, Foods and Medicine. *Appl. Microbiol. Biotechnol.* **2008**, *80*, 1.

(2) Xie, Y.; Jin, Y.; Zeng, X.; Chen, J.; Lu, Y.; Jing, K. Fed-Batch Strategy for Enhancing Cell Growth and C-Phycocyanin Production of Arthrospira (Spirulina) Platensis under Phototrophic Cultivation. *Bioresour. Technol.* **2015**, *180*, 281.

(3) Kuddus, M.; Singh, P.; Thomas, G.; Al-Hazimi, A. Recent Developments in Production and Biotechnological Applications of C-Phycocyanin. *Biomed Res. Int.* **2013**, *2013*, 742859.

(4) Chen, C.-Y.; Kao, P.-C.; Tsai, C.-J.; Lee, D.-J.; Chang, J.-S. Engineering Strategies for Simultaneous Enhancement of C-Phycocyanin Production and CO2 Fixation with Spirulina Platensis. *Bioresour. Technol.* **2013**, *145*, 307.

(5) Romay, C.; González, R.; Ledón, N.; Remirez, D.; Rimbau, V. C-Phycocyanin : A Biliprotein with Antioxidant, Anti-Inflammatory and Neuroprotective Effects. *Curr. Protein Pept. Sci.* **2003**, *4*, 207.

(6) Chen, H.-B.; Wu, J.-Y.; Wang, C.-F.; Fu, C.-C.; Shieh, C.-J.; Chen, C.-I.; Wang, C.-Y.; Liu, Y.-C. Modeling on Chlorophyll a and Phycocyanin Production by Spirulina Platensis under Various Light-Emitting Diodes. *Biochem. Eng. J.* **2010**, *53*, 52.

(7) Feng, C.; Yiming, Z.; Siyuan, G. Growth and Phycocyanin Formation of Spirulina Platensis in Photoheterotrophic Culture. *Biotechnol. Lett.* **1996**, *18*, 603.

(8) Zhang, X.-W.; Zhang, Y.-M.; Chen, F. Kinetic Models for Phycocyanin Production by High Cell Density Mixotrophic Culture of the Microalga Spirulina Platensis. *J. Ind. Microbiol. Biotechnol.* **1998**, *21*, 283.

(9) Radmann, E. M.; Reinehr, C. O.; Costa, J. a. V. Optimization of the Repeated Batch Cultivation of Microalga Spirulina Platensis in Open Raceway Ponds. *Aquaculture.* **2007**, *265*, 118.

(10) Kim, C.-J.; Jung, Y.-H.; Ko, S.-R.; Kim, H.-I.; Park, Y.-H.; Oh, H.-M. Raceway Cultivation of Spirulina Platensis Using Underground Water. *J. Microbiol. Biotechnol.* **2007**, *17*, 853.

(11) Nagy, Z. K. Model Based Control of a Yeast Fermentation Bioreactor Using Optimally Designed Artificial Neural Networks. *Chem. Eng. J.* **2007**, *127*, 95.

(12) Grüne, L.; Pannek, J. Nonlinear Model Predictive Control. In *Nonlinear Model Predictive Control*; **2011**; pp 67–85.

(13) Alagesan, S.; Gaudana, S. B.; Krishnakumar, S.; Wangikar, P. P. Model Based Optimization of High Cell Density Cultivation of Nitrogen-Fixing Cyanobacteria. *Bioresour. Technol.* **2013**, *148*, 228.

(14) Arpornwichanop, A.; Shomchoam, N. Control of Fed-Batch Bioreactors by a Hybrid on-Line Optimal Control Strategy and Neural Network Estimator. *Neurocomputing* **2009**, *72*, 2297.

(15) Mailleret, L.; Bernard, O.; Steyer, J.-P. Nonlinear Adaptive Control for Bioreactors with Unknown Kinetics. *Automatica* **2004**, *40*, 1379.

(16) Oliveira, M. A. C. L. de; Monteiro, M. P. C.; Robbs, P. G.; Leite, S. G. F. Growth and Chemical Composition of Spirulina Maxima and Spirulina Platensis Biomass at Different Temperatures. *Aquac. Int.* **1999**, *7*, 261.

(17) Zhang, D.; Xiao, N.; Mahbubani, K. T.; del Rio-Chanona, E. a.; Slater, N. K. H.; Vassiliadis, V. S. Bioprocess Modelling of Biohydrogen Production by Rhodopseudomonas Palustris: Model Development and Effects of Operating Conditions on Hydrogen Yield and Glycerol Conversion Efficiency. *Chem. Eng. Sci.* **2015**, *130*, 68.

(18) Béchet, Q.; Chambonnière, P.; Shilton, A.; Guizard, G.; Guieysse, B. Algal Productivity Modeling: A Step toward Accurate Assessments of Full-Scale Algal Cultivation. *Biotechnol. Bioeng.* **2015**, *112*, 987.

(19) Zhang, D.; Dechatiwongse, P.; Del-Rio-Chanona, E. A.; Hellgardt, K.; Maitland, G. C.; Vassiliadis, V. S. Analysis of the Cyanobacterial Hydrogen Photoproduction Process via Model Identification and Process Simulation. *Chem. Eng. Sci.* **2015**, *128*, 130.

(20) Aiba, S. Growth Kinetics of Photosynthetic Microorganisms. *Adv. Biochem. Eng.* **1982**, *23*, 85.

(21) Zhang, D.; Dechatiwongse, P.; Hellgardt, K. Modelling Light Transmission, Cyanobacterial Growth Kinetics and Fluid Dynamics in a Laboratory Scale Multiphase Photo-Bioreactor for Biological Hydrogen Production. *Algal Res.* **2015**, *8*, 99.

(22) Zhang, D.; Del-Rio Chanona, E. A.; Vassiliadis, V. S.; Tamburic, B. Analysis of Green Algal Growth via Dynamic Model Simulation and Process Optimization. *Biotechnol. Bioeng.* **2015**, *112*, 2025.

(23) Wächter, A.; Biegler, L. T. On the Implementation of an Interior-Point Filter Line-Search Algorithm for Large-Scale Nonlinear Programming. *Math. Program.* **2006**, *106*, 25.

(24) Hart, W. E.; Laird, C.; Watson, J.-P.; Woodruff, D. L. *Pyomo – Optimization Modeling in Python*; Springer Optimization and Its Applications; Springer US: Boston, MA, **2012**; Vol. 67.

(25) Del Río-Chanona, E. A.; Dechatiwongse, P.; Zhang, D.; Maitland, G.; Hellgardt, K.; Arellano-Garcia, H.; Vassiliadis, V. S. Optimal Operation Strategy for Biohydrogen Production. *Ind. Eng. Chem. Res.* **2015**, *54*, 6334.

(26) Zhang, D.; Dechatiwongse, P.; del Rio-Chanona, E. A.; Maitland, G. C.; Hellgardt, K.; Vassiliadis, V. S. Modelling of Light and Temperature Influences on Cyanobacterial Growth and Biohydrogen Production. *Algal Res.* **2015**, *9*, 263.

(27) Zhang, D.; Dechatiwongse, P.; del Rio-Chanona, E. A.; Maitland, G. C.; Hellgardt, K.; Vassiliadis, V. S. Dynamic Modelling of High Biomass Density Cultivation and Biohydrogen Production in Different Scales of Flat Plate Photobioreactors. *Biotechnol. Bioeng.*, **2015**, in press, doi: 10.1002/bit.25661.

(28) Xie, Y.; Ho, S.-H.; Chen, C.-N. N.; Chen, C.-Y.; Ng, I.-S.; Jing, K.-J.; Chang, J.-S.; Lu, Y. Phototrophic Cultivation of a Thermo-Tolerant Desmodesmus Sp. for Lutein Production: Effects of Nitrate Concentration, Light Intensity and Fed-Batch Operation. *Bioresour. Technol.* **2013**, *144*, 435.

Table 1: Parameters in the Monod model.

Parameter	Value	Parameter	Value
u_m [h^{-1}]	0.0923	k_s [μmol m^{-2} s^{-1}]	178.85
u_d [h^{-1}]	0.0	k_i [μmol m^{-2} s^{-1}]	447.12
K_N [mg L^{-1}]	393.10	k_{sp} [μmol m^{-2} s^{-1}]	23.51
$Y_{NO_3/X}$ [mg g^{-1}]	504.49	k_{ip} [μmol m^{-2} s^{-1}]	800.0
k_m [mg g^{-1} h^{-1}]	2.544	τ [m^2 g^{-1}]	0.0520
k_d [h^{-1}]	0.281	K_a [m^{-1}]	0.0
K_{Np} [mg L^{-1}]	16.89		

Table 2: Parameters in the Droop model.

Parameter	Value	Parameter	Value
u_m [h^{-1}]	0.154	k_i [μmol m^{-2} s^{-1}]	291.54
u_d [h^{-1}]	0.0041	k_{sp} [μmol m^{-2} s^{-1}]	2.309
K_N [mg L^{-1}]	271.59	k_{ip} [μmol m^{-2} s^{-1}]	5000.0
$Y_{NO_3/X}$ [mg g^{-1}]	347.42	τ [m^2 g^{-1}]	0.0761
k_m [mg g^{-1} h^{-1}]	1.528	K_a [m^{-1}]	10.0
k_d [h^{-1}]	1.316	$Y_{q/X}$ [g^{-1}]	0.612
k_s [μmol m^{-2} s^{-1}]	116.62	k_q	1.0

Figure 1: Simulation results of the batch processes. (a) and (b): biomass concentration when incident light intensity is 150 μmol m^{-2} s^{-1} and 300 μmol m^{-2} s^{-1}, respectively; (c) and (d): nitrate concentration when incident light intensity is 150 μmol m^{-2} s^{-1} and 300 μmol m^{-2} s^{-1}, respectively; (e) and (f): phycocyanin production when incident light intensity is 150 μmol m^{-2} s^{-1} and 300 μmol m^{-2} s^{-1}, respectively. Solid line: simulation results of the Monod model, dashed line: simulation results of the Droop model, open circles: experimental results.

Figure 2: Comparison of simulation and experimental results of fed-batch processes. (a) and (b): biomass concentration of the 5 mM fed-batch process and the 10 mM fed-batch process, respectively; (c) and (d): nitrate concentration of the 5 mM fed-batch process and the 10 mM fed-batch process, respectively; (e) and (f): phycocyanin production of the 5 mM and the 10 mM nitrate fed-batch process, respectively. Solid line: simulation results of the Monod model, dashed line: simulation results of the Droop model, open circles: experimental results. The sharp increase of nitrate concentration in Figures 2(c) and 2(d) is due to the intermittent addition of nitrate feed to the reactor.

Figure 3: Light intensity, cell growth rate, phycocyanin accumulation rate and phycocyanin production rate at different locations of the photobioreactor. (a): local light intensity; (b): cell growth rate; (c): phycocyanin accumulation rate; (d): phycocyanin production. Solid line: biomass density is 0.355 g L^{-1} (initial concentration); dashed line: biomass density is 1.505 g L^{-1} (the 50^{th} hour); Dot-dashed line: biomass density is 4.947 g L^{-1} (the 200^{th} hour).

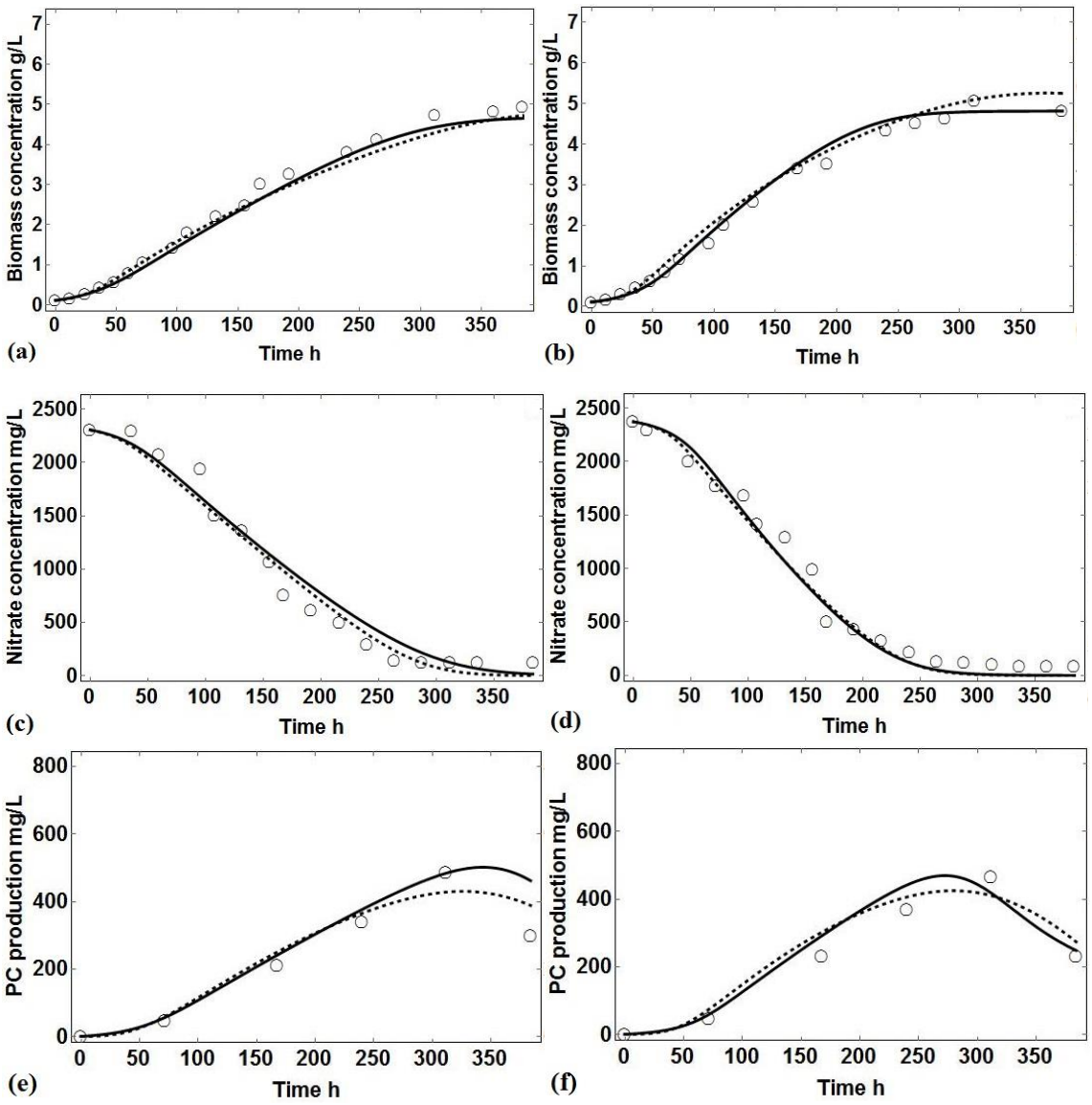

Figure 1: Simulation results of the batch processes. (a) and (b): biomass concentration when incident light intensity is 150 μmol m^{-2} s^{-1} and 300 μmol m^{-2} s^{-1}, respectively; (c) and (d): nitrate concentration when incident light intensity is 150 μmol m^{-2} s^{-1} and 300 μmol m^{-2} s^{-1}, respectively; (e) and (f): phycocyanin production when incident light intensity is 150 μmol m^{-2} s^{-1} and 300 μmol m^{-2} s^{-1}, respectively. Solid line: simulation results of the Monod model, dashed line: simulation results of the Droop model, open circles: experimental results.

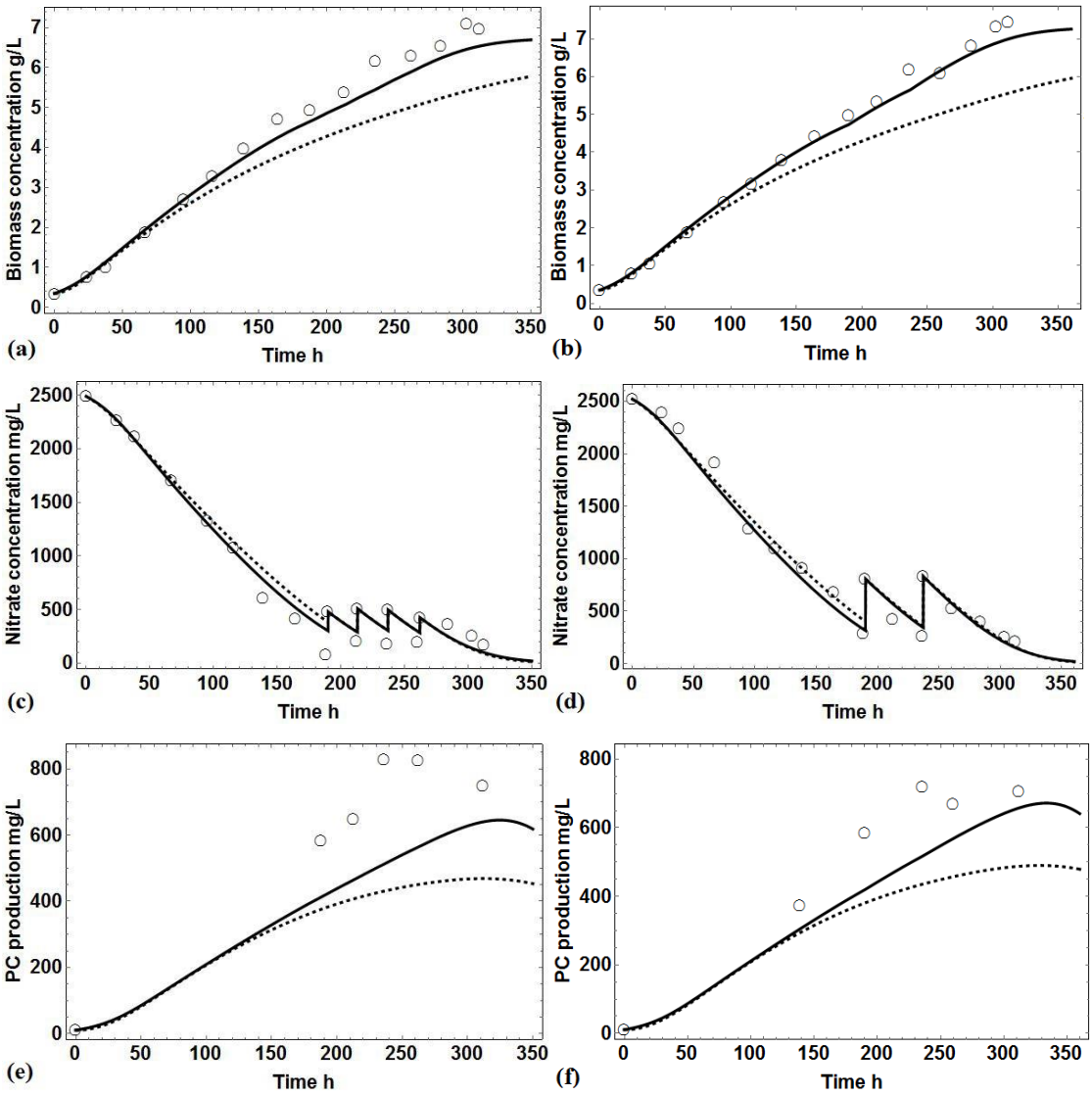

Figure 2: Comparison of simulation and experimental results of fed-batch processes. (a) and (b): biomass concentration of the 5 mM fed-batch process and the 10 mM fed-batch process, respectively; (c) and (d): nitrate concentration of the 5 mM fed-batch process and the 10 mM fed-batch process, respectively; (e) and (f): phycocyanin production of the 5 mM and the 10 mM nitrate fed-batch process, respectively. Solid line: simulation results of the Monod model, dashed line: simulation results of the Droop model, open circles: experimental results. The sharp increase of nitrate concentration in Figures 2(c) and 2(d) is due to the intermittent addition of nitrate feed to the reactor.

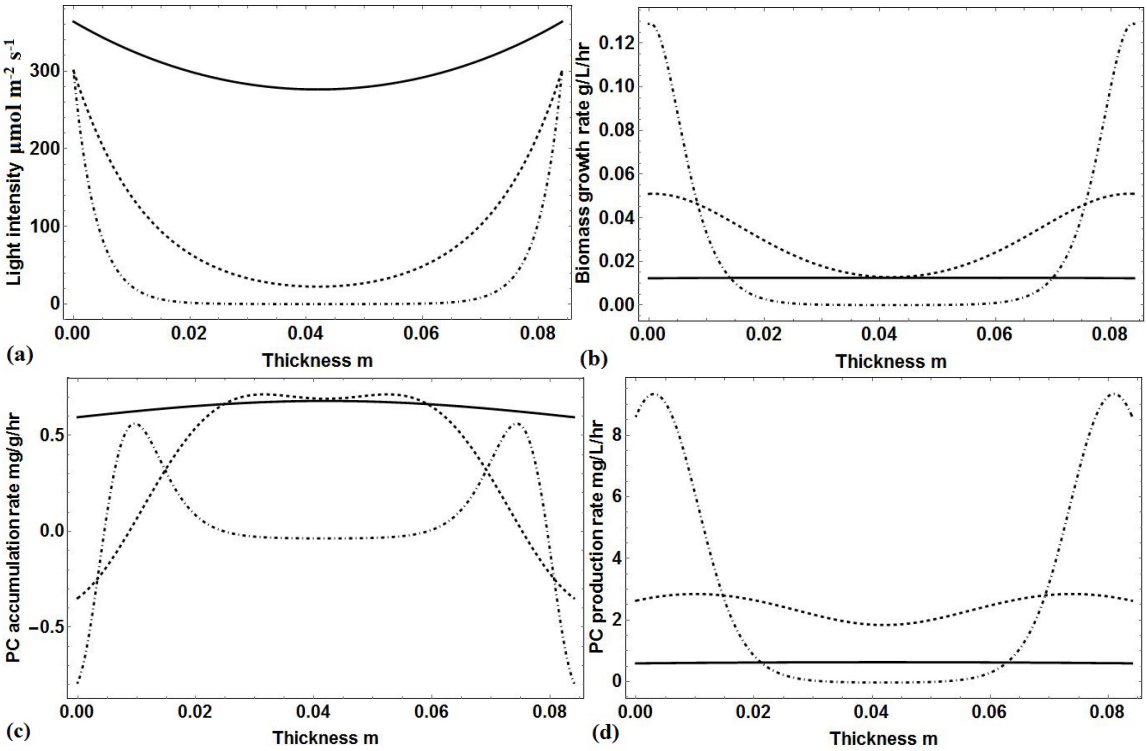

Figure 3: Light intensity, cell growth rate, phycocyanin accumulation rate and phycocyanin production rate at different locations of the photobioreactor. (a): local light intensity; (b): cell growth rate; (c): phycocyanin accumulation rate; (d): phycocyanin production. Solid line: biomass density is 0.355 g L^{-1} (initial concentration); dashed line: biomass density is 1.505 g L^{-1} (the 50^{th} hour); Dot-dashed line: biomass density is 4.947 g L^{-1} (the 200^{th} hour).

For Table of Contents Only